J. Appl. Comput. Mech., 5(4) (2019) 616-626
DOI: 10.22055/JACM.2018.26785.1356

ISSN: 2383-4536
jacm.scu.ac.ir

M&MoCS

Shahid Chamran
University of Ahvaz

Journal of
Applied and Computational Mechanics

Research Paper

The Solar Air Channels: Comparative Analysis, Introduction of Arc-shaped Fins to Improve the Thermal Transfer

Younes Menni[1], Ahmed Azzi[1,2], Ali J. Chamkha[3,4]

[1] Unit of Research on Materials and Renewable Energies, Department of Physics, Faculty of Sciences, Abou Bekr Belkaid University
BP 119-13000-Tlemcen, Algeria

[2] Department of Mechanical Engineering, Faculty of Technology, Abou Bekr Belkaid University
BP 230-13000-Tlemcen, Algeria

[3] Mechanical Engineering Department, Prince Sultan Endowment for Energy and Environment, Prince Mohammad Bin Fahd University
Al-Khobar 31952, Saudi Arabia

[4] RAK Research and Innovation Center, American University of Ras Al Khaimah, United Arab Emirates

Received August 15 2018; Revised October 03 2018; Accepted for publication October 12 2018.
Corresponding author: Younes Menni, menniyounes.cfd@gmail.com
© 2019 Published by Shahid Chamran University of Ahvaz
& International Research Center for Mathematics & Mechanics of Complex Systems (M&MoCS)

Abstract. The problem under investigation contains a computational simulation of a specific heat exchanger with complex geometry fins. The problem solved is potentially interesting for researchers and engineers working on solar collectors and aerospace industry. It is known that heat transfer enhancement can be achieved by creating longitudinal vortices in the flow. These vortices can be generated by arc-shaped fins, and a computational analysis of such solar air channels is not a simple task. Therefore, we used a present-day commercial CFD code to solve the problem. The mathematical problem including the main equations and their explanation, as well as the numerical procedure was presented. The impact of arc-fins' spacings on streamlines and temperature distributions was completely investigated, as well as the heat transfer rate, pressure drop and thermal enhancement factor. The Nusselt number (Nu) and friction loss (f) values of the solar air channel at AR = 1.321 (aspect ratio of channel width-to-height) and S = Pi/2 are found to be around 11.963% and 26.006%; 21.645% and 40.789%; 26.196% and 50.314%; and 30.322% and 58.355% higher than that with S = 3Pi/4, Pi, 5Pi/4 and 3Pi/2, respectively. Importantly, the arc-fins with Re = 12,000 at S = Pi/2 showed higher thermal enhancement performance than the one at S = 3Pi/4, Pi, 5Pi/4 and 3Pi/2 around 2.530%, 6.576%, 6.615% and 6.762%, respectively. This study contains the information which seems to be important for practical engineers.

Keywords: Solar air channel, Comparative analysis, Introduction of arc-shaped fins, Heat transfer enhancement

1. Introduction

Solar air ducts with baffles and fins are the focus of many modern digital and applied studies. Among them, Demartini et al. [1] numerically and experimentally studied the incompressible flow of air through a rectangular section duct, having two flat deflectors. A commercial CFD technique was used for solving the problem. Nasiruddin and Kamran Siddiqui [2] reported the enhancement of thermal transfer in a two-dimensional duct by inserting a plate. The impact of plate height and inclination on the improvement of thermal transfer was investigated in detail. In this investigation, three various arrangements were analyzed, i.e., vertical plate, upstream inclined pale, and downstream inclined plate. Promvonge et al. [3] conducted a computational analysis of laminar fluid and isotherms in a 3D square duct provided by 45° inclined turbulators on one duct surface. The impacts of turbulators' sizes on the thermal-hydrodynamic fields and friction loss in this same duct were investigated and also compared with the simple turbulator case of flat rectangular form. Liu and Wang [4] showed a novel geometric model of the channel with semiattached ribs. The semiattached rib performance was numerically examined by the software Fluent 6.3 in a flow rate range from 10,000 to 25,000. Five various rib configurations and two different stations were studied. Nuntadusit et al. [5] reported the thermal-aerodynamic behavior of air in a duct fitted with various models of perforated ribs. They studied the impact of the angle of inclination of perforated ribs and a position of hole on the rib geometry. The analysis was simulated at a constant Reynolds number condition, 60,000. The impact of the flow geometry on turbulent transient forced-convection flow in a duct of circular section with baffle-type attachments was experimentally evaluated by Tandiroglu [6]. The effects of baffle spacing and orientation angle were analyzed. Dutta and Hossain [7] experimentally examined the local Nusselt number distributions and the skin friction variations in a duct with perforated and inclined solid deflectors. In this work, a two baffles' combination of same size was employed. The first deflector is mounted at the upper hot wall, while the form, arrangement, and the station of the other deflectors were varied to identify the optimum geometry for improved thermal transfer. Wong et al. [8] presented numerical and experimental analyses to examine the turbulent forced-convection flow of air through a duct of horizontal rectangular section with square-shaped ribs placed on its lower wall. The impact of various inclined perforated-type baffles on the dynamic and thermal aspects in a rectangular cross section duct with various models of vortex generators was numerically and experimentally checked out by Ary et al. [9]. The Re number was varied from 23.000 to 57.000 and the Shear Stress Transport k-ω model of turbulence was employed in the approach to simulate the flow structure. Sripattanapipat et al. [10] numerically analyzed the laminar periodic forced-convection flow characteristics in a 2D duct with hot surfaces fitted by diamond model baffles in a staggered manner. The effect of the variation in the diamond baffle geometry attack angle on fluid flow and thermal transfer in the duct was investigated and the data of this same diamond baffle were also compared with those of the simple obstacle. Kamali and Binesh [11] reported a computer code to measure the turbulent heat transfer flow and pressure loss in a channel of square configuration with different rib forms attached on one surface. The analysis was simulated for various rib forms, namely, triangular, square, and trapezoidal. The considered algorithm and the calculation software were used to report the thermal transfer evolution between two ribs. Sriromreun et al. [12] numerically and experimentally studied the impact of obstacles on thermal transfer rate enhancement in a duct with rectangular form. In this study, the obstacles were attached in a Z-form arranged in series on the heated upper surface, similar to the absorber surface of a solar air duct.

Thianpong et al. [13] experimentally treated the characteristics of heat transfer flow in a duct provided by twisted-rings. The study was provided using twisted-rings with three various ratios of width and three different ratios of spacing for Re numbers varying from 6.000 to 20.000 employing the air-type fluid as a test fluid. An numerical and experimental analysis was reported by Tamna et al. [14] to calculate the thermal transfer and skin friction loss in a solar energy collector provided by multiple V-baffles at various arrangement model and baffles' spacings for the turbulent regime, Re = 4.000-21.000. Menni et al. [15-30] presented the thermal transfer improvement with simple and complex geometry obstacles. In those studies, the impact of the obstacle geometry and arrangement were investigated. Promvonge [31] experimentally reported a study on thermal transfer enhancement through a square channel fitted with 30° V-fins and quadruple counter-twisted tapes. They examined the effect of relative fin height, pitch, and attack angle on the thermo aerodynamic structure of air in the channel. Chamoli [32] applied the Taguchi experimental design method to find the optimum design parameters of the rectangular section duct with V-downstream perforated baffle deflectors. They examined the impacts of the four parameters such as Reynolds number, open area ratio, relative roughness height and relative roughness pitch. Chamoli and Thakur [33] carried out an experimental analysis to investigate the impact of fluid flow and heat transfer characteristics of air in a rectangular cross section channel which is provided by V-downstream perforated baffles. The effects of Reynolds number (Re = 3800 - 19,000), relative roughness height (e/H = 0.285 - 0.6), relative roughness pitch (P/e = 1 - 4= and open area ratio (from 12% to 44%) were presented. Turbulent forced-convection fluid flow behavior was obtained. Numerical, analytical, and/or experimental works [34-45] for Newtonian, non-newtonian, or nano fluid flows in two or three dimensional, simple or complex geometries for laminar or turbulent regimes were reported. In these analyses, various geometry and flow parameters were treated. Kumar et al. [46] experimentally studied the airflow over baffles of various types of arrangements of blockage, i.e., V-type solid blockage, V-type blockage with gap, transverse perforated blockage, V-type perforated blockage, angled perforated blockage. Kumar et al. [47] carried out another experimental study on the discrete multi V blockages in the air passages to find the impact of variation of V-baffle blockage on the dynamic and thermal aspects. Sharma et al. [48] reported the experimental analysis and optimization of the performance of discrete V-baffles in the solar air ducts. The heat transfer rate, skin friction, thermal hydraulic effective efficiency, and collector efficiency were obtained. Kumar et al. [49] experimentally examined the convective fluid mechanic and skin friction structure over discretized broken V-pattern baffle in a solar air duct. Various geometrical parameters were investigated, i.e., gap width and location. Kumar and Kim [50], and Kumar et al. [51] evaluated, through a numerical study, the thermal transfer and momentum behavior of air in solar air heater duct with multi V-type perforated baffles. In the present current computational fluid mechanic analysis, the impact of arc-type baffles and fins attached repeatedly in a solar air channel on streamlines, velocities, dynamic coefficient of pressure, isotherms, convective rate of heat transfer, skin coefficient of friction, and performance factor of thermal enhancement are numerically determined. The arc-geometry baffle type attachments with an angle of attack of flow of value of 45° were placed periodically into the solar air channel at five various longitudinal separation distances of these same arc-obstacles. The arc-baffles' spacings were not been examined previously.

The approach of Finite Volumes (FVs), the algorithm of discretization SIMPLE, the numerical scheme of QUICK, the model of turbulence of standard k-epsilon (k-ε), by means of a computational fluid mechanic technique 'FLUENT', were used for solving our problem under investigation.

2. Flow Geometry under Investigation

The current solar model is a solar air channel of two-dimensional horizontal rectangular cross section (length: L = 0.554 m, height: H = 0.146 m) provided by arc-shaped baffle-type attachment pairs pointing upstream end and mounted on both bottom and top surfaces with a staggered manner as reported in Fig. 1.

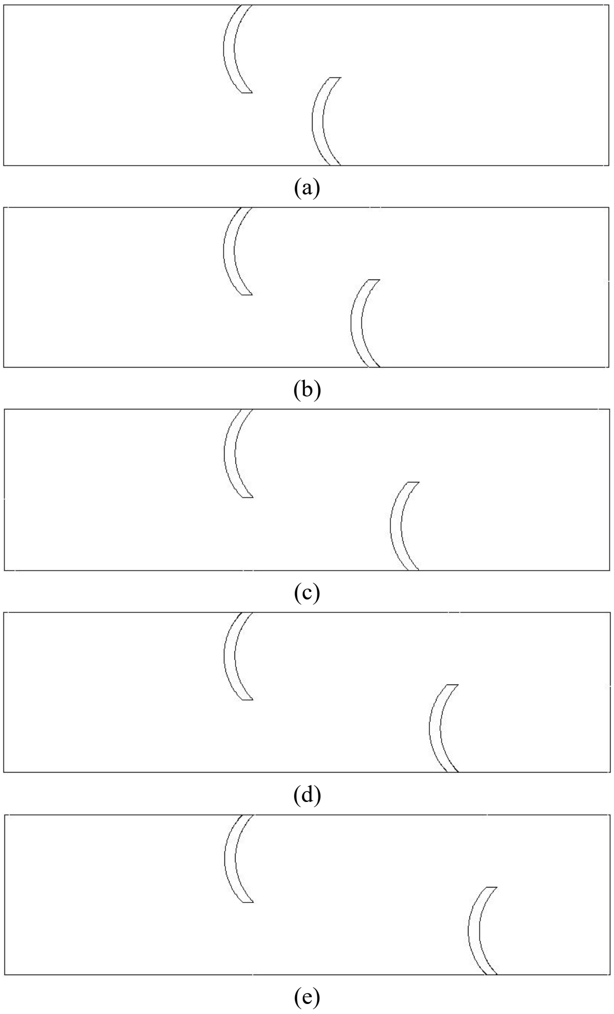

Fig. 1. Geometry under examination for various arc-shaped baffles' spacings: (a) S = Pi/2, (b) S = 3Pi/4, (c) S = Pi, (d) S = 5Pi/4, and (e) S = 3Pi/2

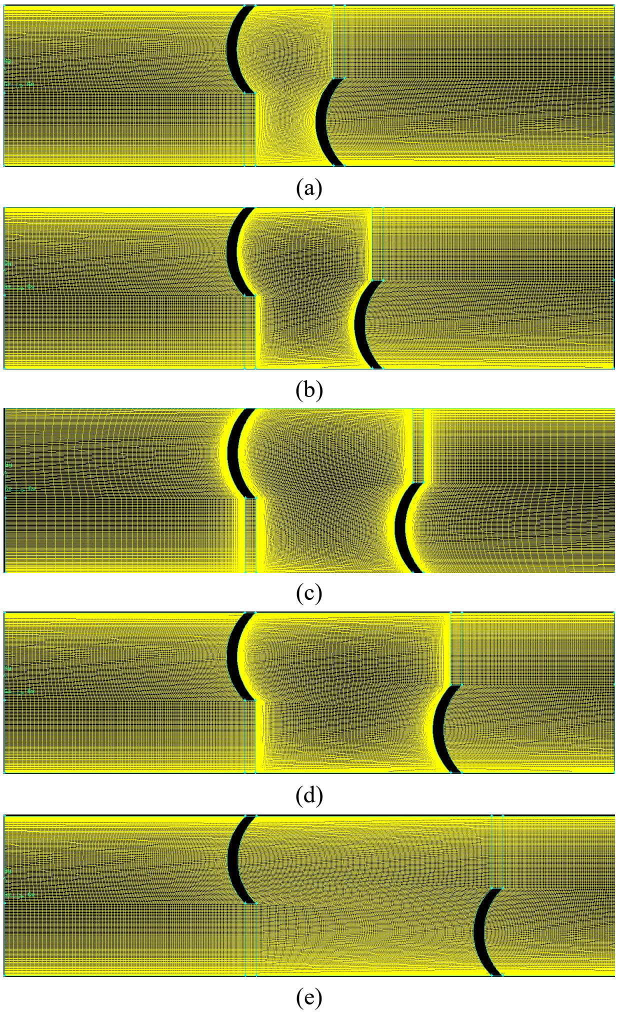

Fig. 2. Mesh generation for different separation distances of arc-shaped baffles: (a) S = Pi/2, (b) S = 3Pi/4, (c) S = Pi, (d) S = 5Pi/4, and (e) S = 3Pi/2

The simulation of computational fluid dynamics in the presence of arc-shaped baffles is conducted under the following conditions: The arc-shaped baffles' attack angle (θ), height (h), and thickness (e) are 45°, 0.08 m, and 0.01 m, respectively. The fluid is 2D, Newtonian (air) and incompressible with constant properties. The heat transfer, and turbulence models are forced-convection, and standard k-epsilon, respectively. The rate of flow in terms of the Reynolds number is constant (Re = 12,000). The axial separation distance (S) between the first and the second arc-shaped baffles is varied from Pi/2 to 3Pi/2 where Pi = 0.142 m as reported this same distance by Demartini et al. [1]. Through these conditions, our mathematical construction of the airflow and forced-convection is governed by:

Equation of continuity:

$$\frac{\partial u_j}{\partial x_j} = 0 \tag{1}$$

Equation of momentum:

$$\rho u_j \frac{\partial u_i}{\partial x_j} = -\frac{\partial P}{\partial x_i} + \frac{\partial}{\partial x_j}\left(\mu \frac{\partial u_i}{\partial x_j} - \rho \overline{u_i^{'} u_j^{'}}\right) \tag{2}$$

Equation of energy:

$$\rho u_j \frac{\partial T}{\partial x_j} = \frac{\partial}{\partial x_j}\left((\Gamma + \Gamma_t)\frac{\partial T}{\partial x_j}\right) \tag{3}$$

Equation of kinetic energy of turbulence:

$$\rho u_j \frac{\partial k}{\partial x_j} = \frac{\partial}{\partial x_j}\left[\left(\mu + \frac{\mu_t}{\sigma_k}\right)\frac{\partial k}{\partial x_j}\right] + G_k - \rho\varepsilon \tag{4}$$

Equation of rate of dissipation of turbulence:

$$\rho u_j \frac{\partial \varepsilon}{\partial x_j} = \frac{\partial}{\partial x_j}\left[\left(\mu + \frac{\mu_t}{\sigma_\varepsilon}\right)\frac{\partial \varepsilon}{\partial x_j}\right] + C_{1\varepsilon}\frac{\varepsilon}{K}G_k - C_{2\varepsilon}\rho\frac{\varepsilon^2}{k} \tag{5}$$

where $C_{1\varepsilon}$, $C_{3\varepsilon}$, $C_{2\varepsilon}$, C_μ, σ_k, σ_ε, and σ_T are the constants of the considered model [52]. The present conditions of boundaries are reported as:

At x=0 and -H/2<y<H/2:

$$u = U_{in} \tag{6a}$$

$$v = 0 \tag{6b}$$

$$T = T_{in} \tag{6c}$$

$$\mathrm{k_{in}} = 0.005\ U_{in}^2 \tag{6d}$$

$$\varepsilon_{in} = 0.1 k_{in}^2 \tag{6e}$$

At $0 \le x \le$ L and y=-H/2 or y=+H/2:

$$u = v = 0 \tag{7a}$$

$$k = \varepsilon = 0 \tag{7b}$$

$$T = T_W \tag{7c}$$

At x=L:

$$\frac{\partial u}{\partial x} = \frac{\partial v}{\partial x} = \frac{\partial T}{\partial x} = \frac{\partial k}{\partial x} = \frac{\partial \varepsilon}{\partial x} = 0 \tag{8a}$$

$$P = P_{atm} \tag{8b}$$

Fluid/solid interface:

$$T_f = T_s \tag{9a}$$

$$\lambda_f \frac{\partial T_f}{\partial n} = \lambda_s \frac{\partial T_s}{\partial n} \tag{9b}$$

where n is the normal coordinate to the wall.

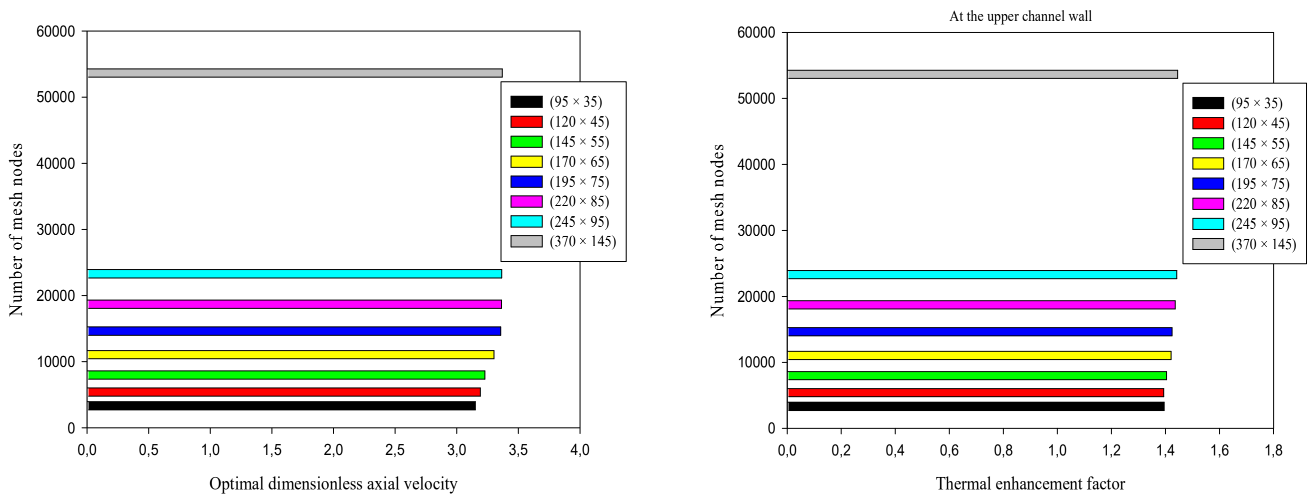

(a) (b)

Fig. 3. Variation of (a) u_{max}/U_{in} and (b) TEF with nodes' density for Re = 12,000

3. Computational Fluid Dynamic Solution

In this analysis, a flow of air is treated. The computational domain is two-dimensional. The solar air channel (SAC) is fitted with hot top and bottom surfaces' placed arc-shaped baffles. The mathematical is governed by continuity, momentum, fluid energy, solid energy, turbulence kinetic energy and turbulence dissipation rate equations. The CFD technique, based on the commercial software FLUENT, is applied to simulate the thermal and aerodynamic fields of air in the SAC. The numerical resolution method of finite volumes [53] is employed to calculate the fluid flow and heat transfer characteristics. The discretization algorithm of SIMPLE-type [53] is used for the pressure-velocity coupling. The numerical scheme of Quick-type is proposed to the interpolations [54]. The numerical scheme of SOU-model [53] is used for the pressure terms. The model of turbulence of k-epsilon version [52] is adopted to describe the phenomenon of turbulence. The mesh is non-uniform, structured, and quadrilateral in both flow x and y directions, Fig. 2. The tests of the independence in the grid are conducted to revel that the solution of the grid independent can be determined. We proposed various mesh cells with the number of nodes varying from 95 to 370, and 35 to 145 along the x and y directions, respectively.

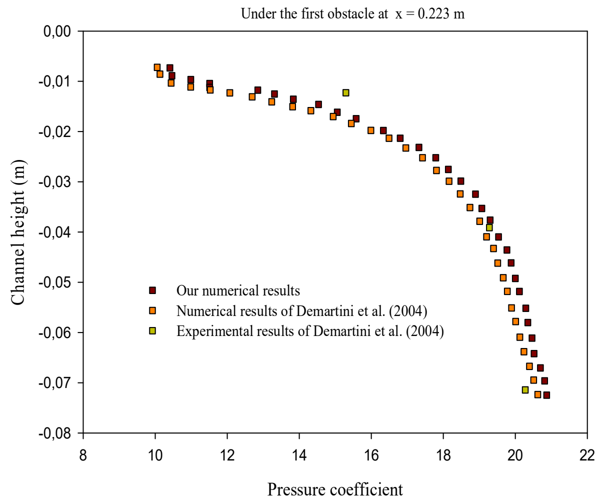

(a)

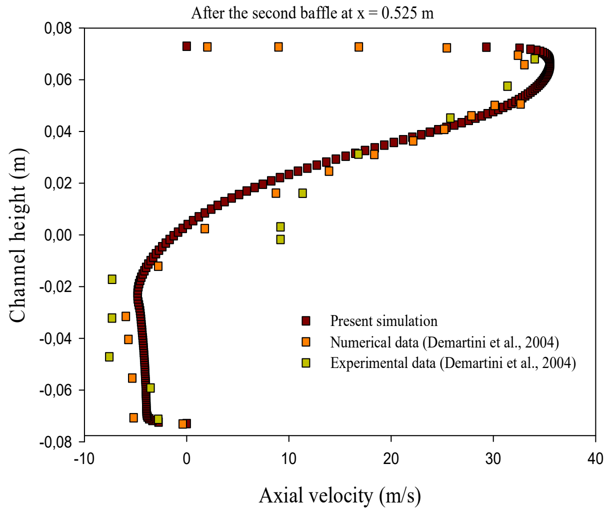

(b)

Fig. 4. Validation of (a) pressure coefficient and (b) axial velocity with the literature

The cell of (245 × 95) reports around 0.150 % and 0.223 % deviation in the optimal dimensionless axial velocity (u_{max}/U_{in}) and the factor of thermal enhancement (TEF), in compared with the 370 × 145 cell, Fig. 3 (a) and (b), respectively. Therefore, the 245 × 95 cell is adopted for the rest of the current computational analysis.
The current numerical data are validated in terms of pressure coefficient (under the first baffle at x = 0.223 m in Fig. 4 (a)) and axial velocity (after the second baffle at x = 0.525 m in Fig. 4 (b)) with the experimental and numerical data obtained by Demartini et al. [1]. For a value of inlet velocity equal to 7.8 m/s (or Re = 8.73 × 104) and as reported on these same figures, a very good concordance is obtained.

4. Results and Discussion

Fig. 5 gives an explanation of the internal structure of the solar channel by highlighting how the distribution of airflow lines starting from the entrance, through the upper and lower fins to the very exit. The air enters at constant axial velocity, of 1.04963 m/s, according to the parallel lines, regular, varying severity. As the first fin approaches, the air current path begins to deform gradually by tilting it towards the bottom of the channel. This extreme deviation causes the creation of a small recycling area, weak in intensity. In the area between the upper and lower fins, the air current is divided into three zones. The first is the main flow of air until it collides with the second obstacle and is turned upwards, forming a recycling area in the front of the bottom fin (second zone). The third area is the movement of the air in reverse, forming a strong rotational loop at the top of the channel behind the first fin. Because of the presence of the second fin and with the help of the strong upper rotation area next to the first fin, the air is forced to move very quickly over the second fin, giving parallel lines to the output end with the formation of a large recycling layer but low-intensity at the bottom of the channel behind the second fin.
As the distance between the fins decreases, the path of the movement decreases. The intensity of the disturbance is increased, forming areas of recycling, strong intensity, behind the first fin, while the size of the recycling area increases beyond the second fin, but it is always weak.
To further clarify, we add the mean velocity fields in terms of distance between the fins (see Fig. 6). The speed values increase over the length of the main motion path from left to right. While the speed decreases next to the upper and lower fins in recycling areas, especially the rear. The velocity values change with the distance between the fins. The velocity values are increased by approximating the second fin of the first fin. The shortest distance corresponds to the highest speed value. The maximal values appear in the case of the smallest distance of value S = Pi on Fig. 6 (a), on the upper left side of the second fin and near the upper surface of the channel near its exit.
In Fig. 7, we highlight the effect of arched fins on dynamic pressure values by changing their separation distance interval. The dynamic-pressure of the air current is reduced in several areas of the channel, including the channel's entrance to the fin's first, as well as the back and front areas next to the fins. The dynamic-pressure values increase with the speed of the flow, especially between the fins at the moment of collisions with the second fin and your hand next to the bottom of the channel's hot top wall. There is an effect of the change of the space on the pressure values and as we noted earlier in the speed fields in Fig. 6. The greater the distance between the fins, the lower the pressure values. The distance S = Pi/2 gives an important effect on the

internal structure of the channel by forming a short and fast path with high pressure values.

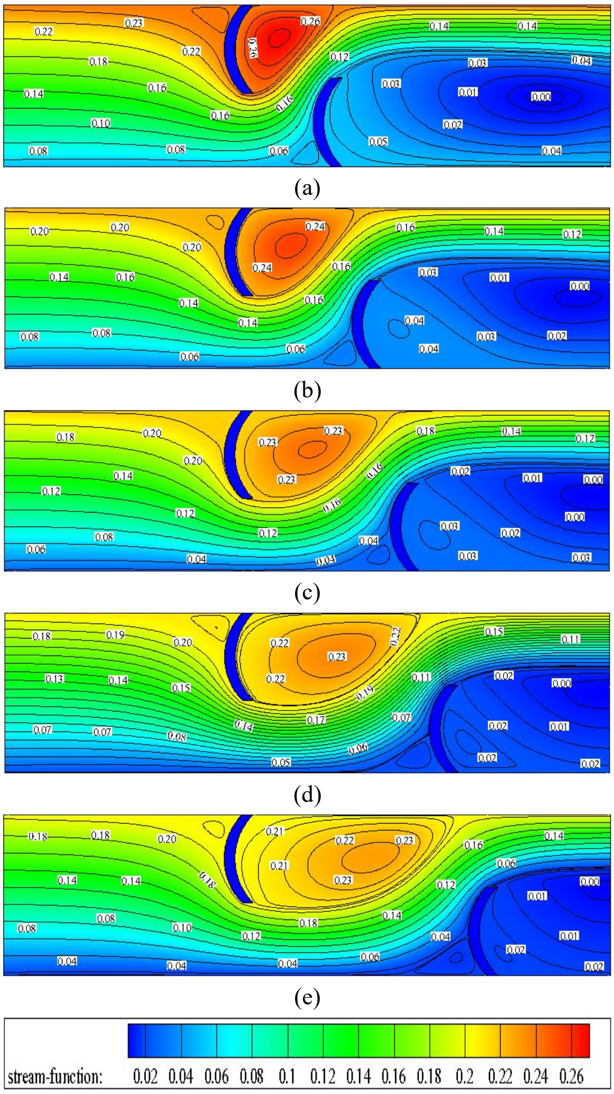

Fig. 5. Variation of streamlines with arc-shaped baffles' separation distance: (a) S = Pi/2, (b) S = 3Pi/4(c) S = Pi, (d) S = 5Pi/4, and (e) S = 3Pi/2.

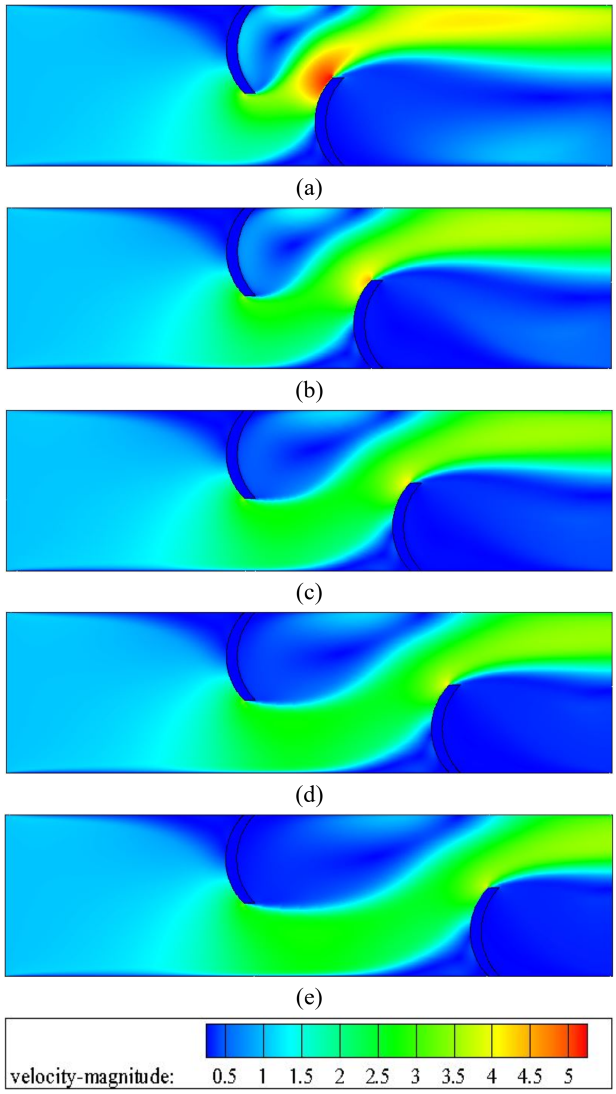

Fig. 6. Variation of mean velocity with arc-shaped baffle spacing: (a) S = Pi/2, (b) S = 3Pi/4, (c) S = Pi, (d) S = 5Pi/4, and (e) S = 3Pi/2.

The complex, irregular, disturbed and heterogeneous structure of airflow has an effective effect on how to distribute the temperature inside the channel, as illustrated in Fig. 8. There is an inverse correlation between flow velocity and fluid temperature in all studied cases. The temperature values of the air molecules in the recycling areas increase, that is, they give good heat exchange between hot walls and fluid. In the areas between the inner walls of the channel and the fins, the temperature drops due to high speed.

Fig. 9 (a) represents the distribution of normalized local Nusselt number (Nu_x/Nu_0) values along the hot top wall of the channel for a fixed value of Reynolds number. The velocity values change by position and airflow area. The Nu_x/Nu_0 values are reduced immediately after the channel entrance until they are not at the level of the first fin position due to the air flows from the upper side of the channel to the lower side through the bottom of the first fin. The Nu_x/Nu_0 values in the recycling area rise behind the first fin due to the large friction with the upper surface until their maximum value reaches the top of the second fin for the moment of the severe collision with the upper surface. The effect of the change of distance between the fins on the velocity values is also shown in this figure. As expected, the Nu_x/Nu_0 values are increased by decreasing the separation distance due to increased flow velocity and severe collision with hot areas.

Fig. 9 (b) gives the changes of normalized skin friction coefficients (Cf/f_0) to the hot top wall of the channel. There are low friction values next to the channel inlet because of the low contact due to the flow of air from the top to the bottom of the channel due to the presence of the first fin. While we observe a significant increase in the Cf/f_0 values behind the first fin due to the concentration of the rear recycling area until it is reduced and is missing due to the end of rotation between the fins. The Cf/f_0 value increases to the highest value of the moment of collision with the upper wall above the second fin due to the latter. The Cf/f_0 coefficient is gradually reduced near the outlet of the channel due to the direction of the flow towards the bottom, as a result of the effective collision with the upper side. The intensity of the friction is increased by increasing the speed of the collision and this is for small intervals.

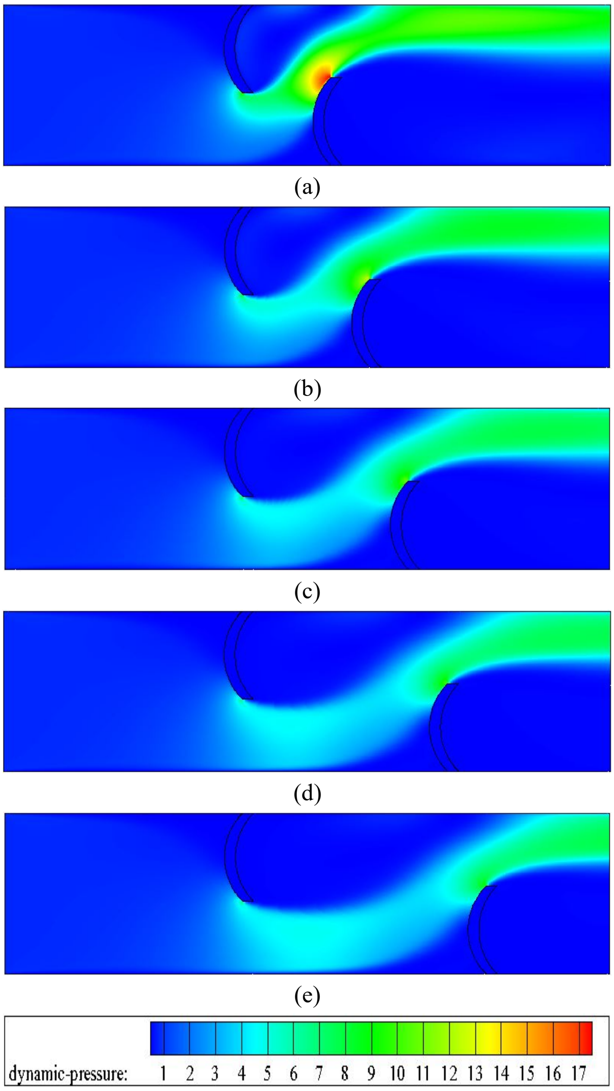

Fig. 7. Variation of coefficient of dynamic-pressure with arc-shaped baffles' separation distance: (a) S = Pi/2, (b) S = 3Pi/4, (c) S = Pi, (d) S = 5Pi/4, and (e) S = 3Pi/2

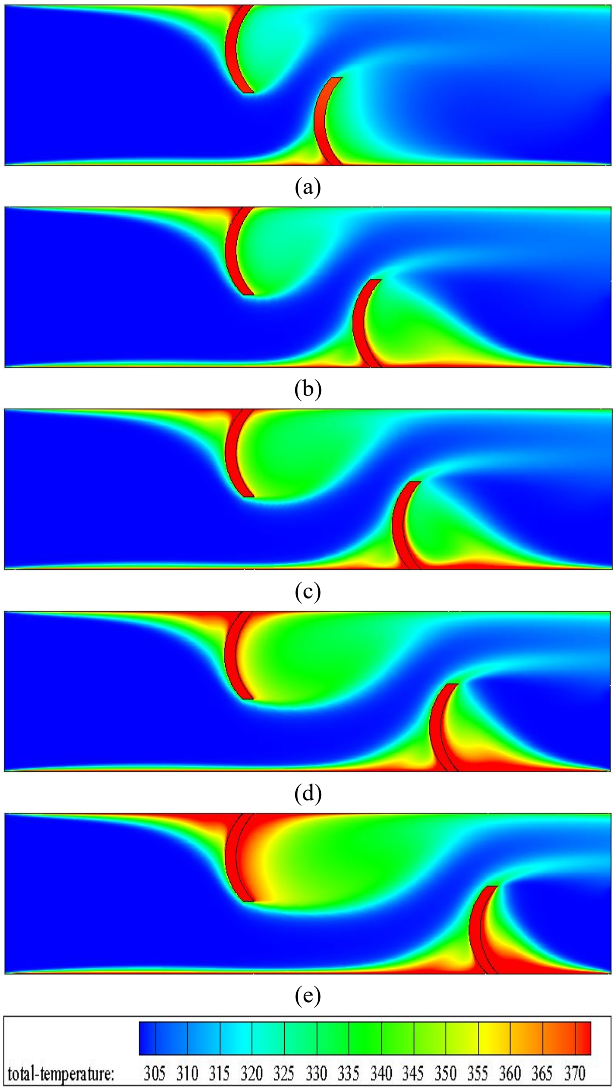

Fig. 8. Variation of isotherms with arc-baffles' spacing: (a) S = Pi/2, (b) S = 3Pi/4, (c) S = Pi, (d) S = 5Pi/4, and (e) S = 3Pi/2

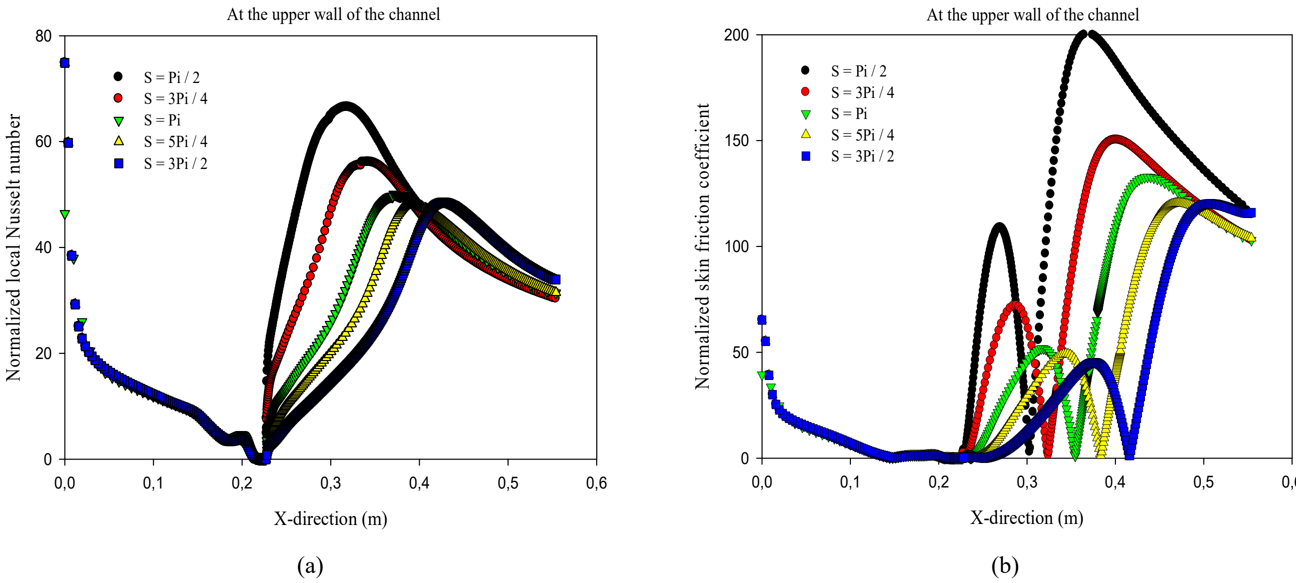

Fig. 9. Variation of normalized (a) local Nusselt number and (b) skin friction coefficient with separation distance of arc-shaped baffles

Fig. 10 (a) and (b) confirms the numerical results of the previous figure (Figs. 9a, and 9b) by highlighting the values of normalized average Nusselt number (Nu/Nu_0) and friction factor (f/f_0). There is an inverse correlation between the length of the axial distance between the fins and the Nu/Nu_0 and f/f_0 values. The distance S = Pi/2 gives high values of Nu/Nu_0 and f/f_0 by 11.963 and 26.006; 21.645 and 40.789; 26.196 and 50.314; and 30.322 and 58.355 percent compared to those given by S = 3Pi/4, Pi, 5Pi/4, and 3Pi/2, respectively. While the longer distance for example S = 3Pi/2 shows a decrease in those transactions by 43.518 and 140.127; 26.349 and 77.679; 12.453 and 42.179; and 5.922 and 19.308 per cent compared to those smaller distances, i.e., S = Pi/2, 3Pi/4, Pi, and 5Pi/4, respectively.

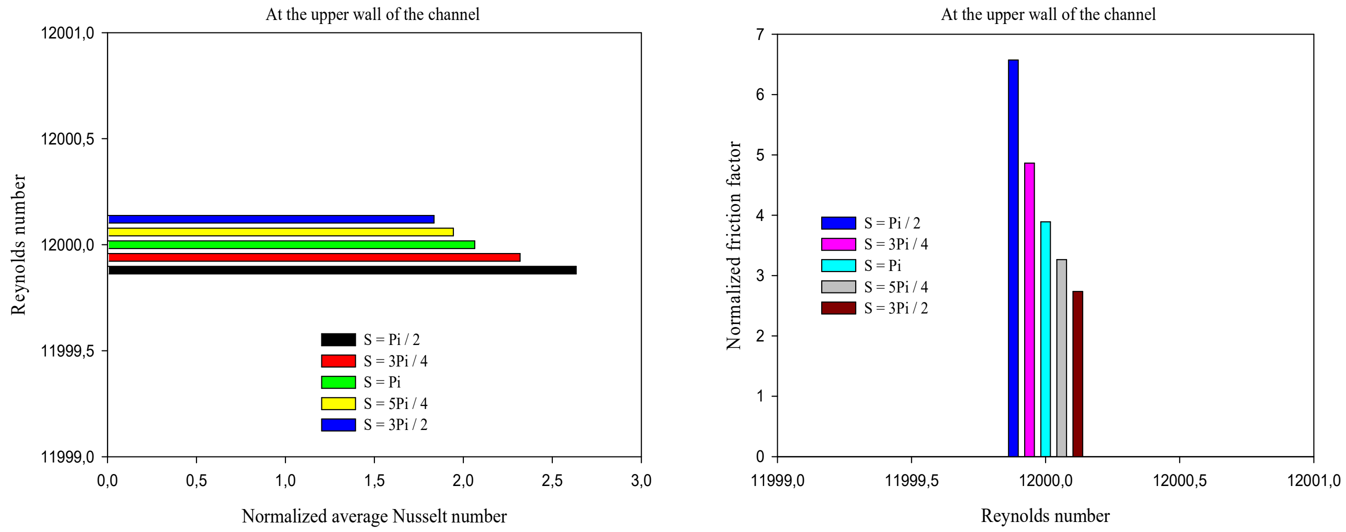

(a) (b)

Fig. 10. Variation of normalized (a) average Nusselt number and (b) friction factor with spacing of arc-shaped baffles.

Fig. 11 shows that the thermal enhancement factor (TEF) values are increased by increasing the S interval values. In all studied cases, TEF values are greater than one. This means that all cases give a dynamic and thermal improvement to the solar channel with arc-fins compared to the solar channel that does not contain fins. Among the most important situations in this area of distances are S = Pi/2. This distance gives optimal performance. This separation shows an improvement of 2.530, 6.576, 6.615, and 6.762 percent compared to those distances S = 3Pi/4, Pi, 5Pi/4, and 3Pi/2, respectively.

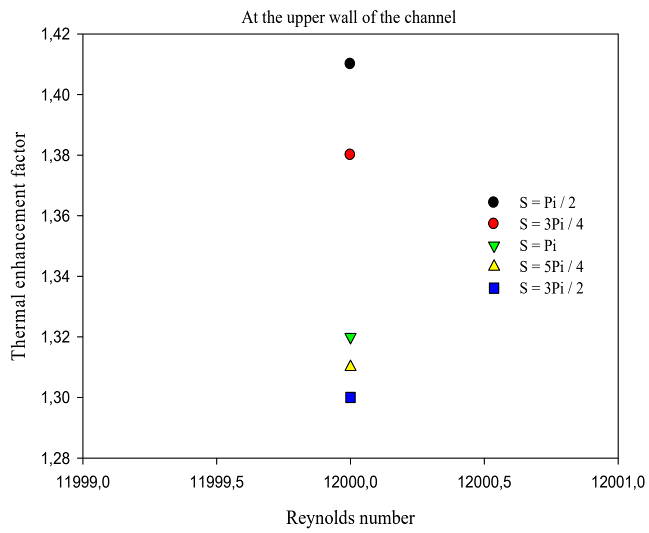

Fig. 11. Variation of thermal enhancement factor with arc-baffle spacing

So, insert the arched fins inside the solar air channel at a sharp angle of 45° and a minimum separation distance of S = Pi/2 is the perfect solution for thermal and dynamic best for this topic channel performance.

5. Conclusion

This study was numerical for turbulent airflow within a solar channel containing arched fins of different spacings. Various key points are as follows:

- A complex, irregular, disturbed and heterogeneous structure of the channel internally.
- The airflow is composed of two different currents: the first is main, from left to right, while the second is in the opposite direction in front and behind each fin and the representative in the recycling areas.
- Recycling areas are characterized by low speed and high temperature.
- The decrease in the distance between the arched fins increases the severity of the collision between the aerobic particles and the hot areas by creating frictions and thus better heat exchange.

- For better efficiency, we enter the arched fins inside the solar air channel with small spaces such as S = Pi/2. This distance shows an increase in performance by 2.530, 6.576, 6.615, and 6.762 percent compared to those given by S = 3Pi/4, Pi, 5Pi/4, and 3Pi/2, respectively.

Conflict of Interest

The author(s) declared no potential conflicts of interest with respect to the research, authorship and publication of this article.

Funding

The author(s) received no financial support for the research, authorship and publication of this article.

Nomenclature

Cf	Skin friction coefficient	P_{atm}	Atmospheric pressure, Pa
$C_{1\varepsilon}$	Constant used in the standard K-ε model	Pr	Molecular Prandtl number
$C_{2\varepsilon}$	Constant used in the standard K-ε model	Pr_t	Turbulent Prandtl number
C_μ	Constant used in the standard K-ε model	Re	Reynolds number based on the channel hydraulic diameter
G_k	Production of turbulent kinetic energy, m^2/s^2	T	Temperature, °C
H	Channel height, m	T_{in}	Inlet temperature, °C
h	Arc-baffle height, m	T_w	Wall temperature, °C
k	Turbulent kinetic energy, m^2/s^2	$\overline{U}$	Mean axial velocity of the section, m/s
L	Length of rectangular channel in x-direction, m	U_{in}	Inlet velocity, m/s
L_{in}	Distance upstream of the first arc-baffle, m	u	Fluid velocity in x-direction, m/s
L_{out}	Distance downstream of the second arc-baffle, m	u_i, u_j	Mean velocity component in x_i-, x_j- direction, m/s
Nu_x	Local Nusselt number	u'_i, u'_j	Fluctuation velocity component in x_i-, x_j- direction, m/s
ΔP	Pressure drop, Pa	v	Fluid velocity in y-direction, m/s
P	Pressure, Pa	w	Arc-baffle width, m
Pi	Arc-baffle distance or spacing, m	x, y	Cartesian coordinates, m

Greek Symbols

ε	Specific dissipation rate, m^2/s	μ	Molecular viscosity, Kg/m.s
κ	Von Kármán constant, (=0.4187)	μ_t	Eddy viscosity, Kg/m.s
Γ	Molecular thermal-diffusivity, Kg/m.s	σ_k	Turbulent Prandtl number for K-equation
Γ_t	Turbulent thermal-diffusivity, Kg/m.s	σ_ε	Turbulent Prandtl number for ε-equation
δ_{ij}	Kronecker delta	σ_T	Turbulent Prandtl number for energy equation
ρ	Fluid density, kg/m^3	θ	Half attack angle of baffle, degree (°)
λ_f	Fluid thermal conductivity, W/m.°C	τ_w	Wall shear stress, $Kg/s^2.m$
λ_s	Solid thermal conductivity, W/m.°C	ϕ	Stands for the dependent variables u, v, K, ε and T

Subscript

atm	Atmospheric	s	Solid
f	Fluid	t	Turbulent
i, j	Refers coordinate direction vectors	w	Wall
in	Inlet of the computational domain	x	Local
out	Outlet of the computational domain		

References

[1] L.C. Demartini, H.A. Vielmo, and S.V Möller, Numeric and experimental analysis of the turbulent flow through a channel with baffle plates, *Journal of Brazilian Society of Mechanical Sciences and Engineering*, 26(2), 2004, pp. 153-159.
[2] Nasiruddin, and M.K. Kamran Siddiqui, Heat transfer augmentation in a heat exchanger tube using a baffle, *International Journal of Heat and Fluid Flow*, 28(2), 2007, pp. 318-328.
[3] P. Promvonge, S. Sripattanapipat, and S. Kwankaomeng, Laminar periodic flow and heat transfer in square channel with 45° inline baffles on two opposite walls, *International Journal of Thermal Sciences*, 49, 2010, pp. 963-975.
[4] H. Liu, and J. Wang, Numerical investigation on synthetical performances of fluid flow and heat transfer of semi attached rib-channels, *International Journal of Heat and Mass Transfer*, 54, 2011, pp. 575-583.
[5] C. Nuntadusit, M. Wae-hayee, A. Bunyajitradulya, and S. Eiamsaard, Thermal visualization on surface with transverse perforated ribs, *International Communications in Heat and Mass Transfer*, 39, 2012, pp. 634-639.
[6] A. Tandiroglu, Effect of flow geometry parameters on transient heat transfer for turbulent flow in a circular tube with baffle inserts, *International Journal of Heat and Mass Transfer*, 49, 2006, pp. 1559-1567.
[7] P. Dutta, and A. Hossain, Internal cooling augmentation in rectangular channel using two inclined baffles, *International*

Journal of Heat and Fluid Flow, 26, 2005, pp. 223-232.
[8] T.T. Wong, C.W. Leung, Z.Y. Li, and W.Q. Tao, Turbulent convection of air-cooled rectangular duct with surface-mounted cross-ribs, *International Journal of Heat and Mass Transfer*, 46, 2003, pp. 4629-4638.
[9] B.K.P. Ary, M.S. Lee, S.W. Ahn, and D.H. Lee, The effect of the inclined perforated baffle on heat transfer and flow patterns in the channel, *International Communications in Heat and Mass Transfer*, 39, 2012, pp. 1578-1583.
[10] S. Sripattanapipat, and P. Promvonge, Numerical analysis of laminar heat transfer in a channel with diamond-shaped baffles, *International Communications in Heat and Mass Transfer*, 36, 2009, pp. 32-38.
[11] R. Kamali, and A.R. Binesh, The importance of rib shape effects on the local heat transfer and flow friction characteristics of square ducts with ribbed internal surfaces, *International Communications in Heat and Mass Transfer*, 35, 2008, pp. 1032-1040.
[12] P. Sriromreun, C. Thianpong, and P. Promvonge, Experimental and numerical study on heat transfer enhancement in a channel with Z-shaped baffles, *International Communications in Heat and Mass Transfer*, 39, 2012, pp. 945-952.
[13] C. Thianpong, K. Yongsiri, K. Nanan, and S. Eiamsa-ard, Thermal performance evaluation of heat exchangers fitted with twisted-ring turbulators, *International Communications in Heat and Mass Transfer*, 39, 2012, pp. 861-868
[14] S. Tamna, S. Skullong, C. Thianpong, and P. Promvonge, Heat transfer behaviors in a solar air heater channel with multiple V-baffle vortex generators, *Solar Energy*, 110, 2014, pp. 720-735.
[15] Y. Menni, A. Azzi, C. Zidani, and B. Benyoucef, Numerical analysis of turbulent forced-convection flow in a channel with staggered l-shaped baffles, *Journal of New Technology and Materials*, 6(2), 2016, pp. 44-55.
[16] Y. Menni, A. Azzi, and C. Zidani, Use of waisted triangular-shaped baffles to enhance heat transfer in a constant temperature-surfaced rectangular channel, *Journal of Engineering Science and Technology*, 12(12), 2017, pp. 3251-3273.
[17] Y. Menni, A. Azzi, F. Didi, and S. Harmand, Computational fluid dynamical analysis of new obstacle design and its impact on the heat transfer enhancement in a specific type of air flow geometry, *Computational Thermal Sciences*, 10(5), 2018, pp. 421-447.
[18] Y. Menni, and A. Azzi, Computational fluid dynamical analysis of turbulent heat transfer in a channel fitted with staggered v-shaped baffles, *World Journal of Modelling and Simulation*, 14(2), pp. 108-123.
[19] Y. Menni, and A. Azzi, Numerical analysis of thermal and aerodynamic fields in a channel with cascaded baffles, *Periodica Polytechnica Mechanical Engineering*, 62(1), 2018, 16-25.
[20] Y. Menni, and A. Azzi, Effect of fin spacing on turbulent heat transfer in a channel with cascaded rectangular-triangular fins, *Journal of New Technology and Materials*, 7(2), 2017, pp. 10-21.
[21] Y. Menni, and A. Azzi, Design and performance evaluation of air solar channels with diverse baffle structures, *Computational Thermal Sciences*, 10(3), 2018, pp. 225-249.
[22] Y. Menni, A. Azzi, and A.J. Chamkha, Enhancement of convective heat transfer in smooth air channels with wall-mounted obstacles in the flow path, *Journal of Thermal Analysis and Calorimetry*, 2018, https://doi.org/10.1007/s10973-018-7268-x.
[23] Y. Menni, A. Azzi, and A.J. Chamkha, Aerodynamics and heat transfer over solid-deflectors in transverse, staggered, corrugated-upstream and corrugated-downstream patterns, *Periodica Polytechnica Mechanical Engineering*, 62(3), 2018, pp. 209-217.
[24] Y. Menni, A.J. Chamkha, and A. Azzi, Nanofluid Transport in Porous Media - A Review, *Special Topics & Reviews in Porous Media*, 2018, doi: 10.1615/SpecialTopicsRevPorousMedia.2018027168
[25] Y. Menni, A. Azzi, and C. Zidani, Etude numérique comparative entre deux types de chicanes et ailettes (rectangulaire et rectangulaire arrondie) utilisées pour améliorer les performances des capteurs solaires plans à air, *Revue des Energies Renouvelables*, 18(3), 2015, pp. 347-361.
[26] Y. Menni, A. Azzi, C. Zidani, and B. Benyoucef, Low-Reynolds-number turbulent forced-convection flow over graded baffle plates, *Revue des Energies Renouvelables*, 19(2), 2016, pp. 235-250.
[27] Y. Menni, A. Azzi, and C. Zidani, Computational analysis of heat transfer and fluid flow characteristics over flat bars of different heights, *Revue des Energies Renouvelables*, 19(3), 2016, pp. 345-366.
[28] Y. Menni, A. Azzi, and C. Zidani, Computational analysis of turbulent forced convection in a channel with staggered corrugated baffles, *Communication Science & Technology*, 16, 2016, pp. 34-43.
[29] Y. Menni, A. Azzi, and C. Zidani, Numerical study of turbulent heat transfer in a trapezoïdal channel with flat baffles, *Communication Science & Technology*, 17, 2016, pp. 67-77.
[30] Y. Menni, A. Azzi, and C. Zidani, Contribution numérique à l'étude bidimensionnelle de la convection forcée turbulente dans un canal horizontal muni des chicanes transversales sous forme rectangulaire arrondie, *Revue des Sciences et Sciences de l'Ingénieur*, 6(1), 2016, pp. 17-26.
[31] P. Promvonge, Thermal performance in square-duct heat exchanger with quadruple V-finned twisted tapes, *Applied Thermal Engineering*, 91, 2015, pp. 298-307.
[32] S. Chamoli, A Taguchi approach for optimization of flow and geometrical parameters in a rectangular channel roughened with V down perforated baffles, *Case Studies in Thermal Engineering*, 5, 2015, pp. 59-69.
[33] S. Chamoli, and N.S. Thakur, Correlations for solar air heater duct with V-shaped perforated baffles as roughness elements on absorber plate, *International Journal of Sustainable Energy*, 2013, http://dx.doi.org/10.1080/14786451.2013.857318
[34] A.R. Noghrehabadi, A. Behseresht, M. Ghalambaz, and J. Behseresht, Natural-convection flow of nanofluids over vertical cone embedded in non-darcy porous media, *Journal of Thermophysics and Heat Transfer*, 27, 2013, pp. 334-341.
[35] A.R. Noghrehabadi, R. Pourrajab, and M. Ghalambaz, Effect of partial slip boundary condition on the flow and heat transfer of nanofluids flow past stretching sheet prescribed constant wall temperature, *International Journal of Thermal Sciences*, 54, 2012, pp. 253-261.

[36] A.R. Noghrehabadi, R. Pourrajab, and M. Ghalambaz, Flow and heat transfer of nanofluids over stretching sheet taking into account partial slip and thermal convective boundary conditions, *Heat and Mass Transfer*, 49, 2013, pp. 1357-1366.
[37] A.R. Noghrehabadi, M.R. Saffarian, R. Pourrajab, and M. Ghalambaz, Entropy analysis for nanofluid flow over a stretching sheet in the presence of heat generation/absorption and partial slip, *Journal of Mechanical Science and Technology*, 27, 2013, pp. 927-937.
[38] M. Ghalambaz, A. Doostanidezfouli, E. Izadpanahi, and A.J. Chamkha, Phase- change heat transfer in a cavity heated from below: the effect of utilizing single or hybrid nanoparticles as additives, *Journal of the Taiwan Institute of Chemical Engineers*, 72, 2017, pp. 104-115.
[39] A.J. Chamkha, and J. Al-Humoud, Mixed convection heat and mass transfer of non-newtonian fluids from a permeable surface embedded in a porous medium, *International Journal of Numerical Methods for Heat & Fluid Flow*, 17, 2007, pp. 195-212.
[40] A.J. Chamkha, and A.-R.A. Khaled, Similarity solutions for hydromagnetic mixed convection heat and mass transfer for Hiemenz flow through porous media, *International Journal of Numerical Methods for Heat & Fluid Flow*, 10, 2000, pp. 94-115.
[41] A.J. Chamkha, and A.M. Rashad, Natural convection from a vertical permeable cone in a nanofluid saturated porous media for uniform heat and nanoparticles volume fraction fluxes, *International Journal for Numerical Methods in Heat and Fluid Flow*, 22, 2012, pp. 1073-1085.
[42] A.J. Chamkha, S.M.M. EL-Kabeir, and A.M. Rashad, Heat and mass transfer by non-darcy free convection from a vertical cylinder embedded in porous media with a temperature-dependent viscosity, *International Journal for Numerical Methods in Heat and Fluid Flow*, 21, 2011, pp.847-863.
[43] A.J. Chamkha, A. Doostanidezfuli, E. Izadpanahi, and M. Ghalambaz, Phase- change heat transfer of single/hybrid nanoparticles-enhanced phase-change materials over a heated horizontal cylinder confined in a square cavity, *Advanced Powder Technology*, 28, 2017, pp. 385-397.
[44] A.J. Chamkha, Non-similar solutions for heat and mass transfer by hydromagnetic mixed convection flow over a plate in porous media with surface suction or injection, *International Journal of Numerical Methods for Heat & Fluid Flow*, 10, 2000, pp. 142-162.
[45] A.J. Chamkha, Unsteady laminar hydromagnetic flow and heat transfer in porous channels with temperature-dependent properties, *International Journal of Numerical Methods for Heat & Fluid Flow*, 11, 2001, pp. 430-448.
[46] R. Kumar, A. Kumar, R. Chauhan, and R. Maithani, Comparative study of effect of various blockage arrangements on thermal hydraulic performance in a roughened air passage, *Renewable and Sustainable Energy Reviews*, 81, 2018, pp. 447-463.
[47] A. Kumar, R. Chauhan, R. Kumar, T. Singh, M. Sethi, A. Kumar, A. Sharma, Developing heat transfer and pressure loss in an air passage with multi discrete V-blockages, *Experimental Thermal and Fluid Science*, 84, 2017, pp.266-278.
[48] A. Sharma, R. Chauhan, T. Singh, A. Kumar, R. Kumar, A. Kumar, and M. Sethi, Optimizing discrete V obstacle parameters using a novel Entropy-VIKOR approach in a solar air flow channel, *Renewable Energy*,106 2017, pp.310-320.
[49] R. Kumar, M. Sethi, R. Chauhan, and A. Kumar, Experimental study of enhancement of heat transfer and pressure drop in a solar air channel with discretized broken V-pattern baffle, *Renewable Energy*, 101, 2017, pp. 856-872
[50] R. Kumar, A. Kumar, A. Sharma, R. Chauhan, and M. Sethi, experimental study of heat transfer enhancement in a rectangular duct distributed by multi V‑perforated baffle of different relative baffle width, *Heat and Mass Transfer*, 53, 2017, pp. 1289-1304.
[51] A. Kumar, and M.H. Kim, Thermal hydraulic performance in a solar air heater channel with multi v-type perforated baffles, *Energies*, 9, 2016, pp. 564
[52] B.E. Launder, and D.B. Spalding, The numerical computation of turbulent flows, *Computer Methods Applied Mechanics Eng.*, 3, 1974, pp. 269-289.
[53] S.V. Patankar, Numerical heat transfer and fluid flow, McGraw-Hill, New York, 1980.
[54] B.P. Leonard, and S. Mokhtari, Ultra-sharp nonoscillatory convection schemes for high-speed steady multidimensional flow, NASA TM 1-2568, NASA Lewis Research Center, 1990.

© 2019 by the authors. Licensee SCU, Ahvaz, Iran. This article is an open access article distributed under the terms and conditions of the Creative Commons Attribution-NonCommercial 4.0 International (CC BY-NC 4.0 license) (http://creativecommons.org/licenses/by-nc/4.0/).